Catalysis Science & Technology

Catalytic Oxidation of Propane over Palladium Alloyed with Gold: An Assessment of the Chemical and Intermediate Species

Journal:	*Catalysis Science & Technology*
Manuscript ID	CY-ART-08-2018-001704.R3
Article Type:	Paper
Date Submitted by the Author:	23-Oct-2018
Complete List of Authors:	Kareem, Haval; State University of New York at Binghamton, Chemistry Shan, Shiyao; State University of New York at Binghamton, Department of Chemistry Wu, Zhipeng; State University of New York at Binghamton, Department of Chemistry Velasco, Leslie; State University of New York at, Department of Chemistry Moseman, Kelli; State University of New York at, Department of Chemistry O'Brien, Casey; US Army Research Laboratory Tran, Dat; US Army Research Laboratory Lee, Ivan; U.S. Army Research Laboartory, Sensors and Electron Devices Directorate Maswadeh, Yazan; CMU, Physics Yang, Lefu; Catalysis, Chemistry Mott, Derrick; Tohoku University - Katahira Campus, Institute of Multidisciplinary Research for Advanced Materials Luo, Jin; State University of New York at Binghamton, Department of Chemistry Petkov, Valeri; CMU, Physics Zhong, Chuan-jian; State University of New York at, Department of Chemistry

Catalytic Oxidation of Propane over Palladium Alloyed with Gold: An Assessment of the Chemical and Intermediate Species

Haval Kareem,[a] Shiyao Shan,[a] Zhi-Peng Wu,[a] Leslie Velasco,[a] Kelli Moseman,[a] Casey P. O'Brien, Dat T. Tran, [c]Ivan c. Lee,[c] Yazan Maswadeh,[b] Lefu Yang,[d] Derrick Mott,[e] Jin Luo,[a] Valeri Petkov,[b] and Chuan-Jian Zhong [a,*]

[a)] Department of Chemistry, State University of New York at Binghamton, Binghamton, NY 13902, USA
[b)] Department of Physics, Central Michigan University, Mt. Pleasant, Michigan 48859, USA
[c)] U.S. Army Research Laboratory, Sensors and Electron Devices Directorate, Adelphi, MD 20783, USA
[d)] College of Chemistry and Chemical Engineering, Xiamen University, Xiamen 361005, China
[e)] School of Materials Science, Japan Advanced Institute of Science and Technology, Nomi, Ishikawa 923-1292, Japan

Abstract. Understanding the catalytic oxidation of propane is important for developing catalysts not only for catalytic oxidation of hydrocarbons in emission systems but also for selective oxidation in chemical processing industry. For palladium-based catalysts, little is known about the identification of the chemical or intermediate species involved in propane oxidation. We describe herein findings of an investigation of the catalytic oxidation of propane over supported palladium nanoalloys with different compositions of gold (Pd_nAu_{100-n}), focusing on probing the chemical or intermediate species on the catalysts in correlation with the bimetallic composition and the alloying phase structure. In addition to an enhanced catalytic activity, a strong dependence of the catalytic activity on the bimetallic composition was revealed, displaying an activity maximum at Pd:Au ratio of 50:50 in terms of reaction temperature. This dependence is also reflected by its dependence on the thermochemical treatment condition. While the activity for nanoalloys with n ~50 showed little change after the thermochemical treatment under oxygen, the activities for nanoalloys with n < 50 and n > 50 showed opposite trend. Importantly, this catalytic synergy is linked to the subtle differences of chemical and intermediate species which have been identified for the catalysts with different bimetallic composition by in-situ measurements using Diffuse Reflectance Infrared Fourier Transform Spectroscopy (DRIFTS). For catalytic oxidation of propane over the highly-active catalyst with Pd:Au ratio of 50:50, major species identified include acetate and bicarbonate, showing subtle differences in comparison with the identification of bicarbonate and formate for the catalyst with <50%Au (with a lower activity), and absence of apparent species for the catalyst with >50%Au (largely absent of activity). The alloying of 50% Au in Pd is believed to increase the oxophilicity of Pd, which facilitate the first carbon-carbon bond cleavage and oxygenation of propane. Implications of the findings to catalytic synergy of Pd alloyed with Au and the design of active Pd alloy catalysts are also discussed.

Keywords: Thermochemically-tuned nanoalloys, palladium-gold nanoparticles, support effect, in-situ DRIFTS probing, surface catalytic sites, intermediate species, propane oxidation

Broader context:

The development of effective routes to clean energy production and air pollutant elimination is important for energy and environmental sustainability, in which catalysis plays a central role. A major challenge is the understanding of the catalyst structures and surface sites for the design of active and stable catalysts for the targeted catalytic reactions. One example is the catalytic oxidation of propane, which is important not only for clean fuel production but also for hydrocarbon pollution reduction. However, the current understanding of the catalyst design in terms of specific phase structures and surface sites is very limited. Herein, this work reports novel findings of a study of the catalytic propane oxidation over a nanoalloy catalyst consisting of palladium alloyed with gold, aiming at establishing the correlation among the phase structure, chemical composition, support interaction, and surface sites of the catalysts. In particular, the work focuses on in-situ monitoring of the nanoscale evolution of surface catalytic sites by probing the chemical and intermediate species on the catalyst surfaces in correlation with the structure and activity using advanced and analytical techniques such as synchrotron high-energy X-ray diffraction coupled to atomic pair distribution function analysis and diffuse reflectance infrared Fourier transform spectroscopy. The findings provide a new insight for the design of active and stable nanoalloys for advancing clean energy production and sustainable environment.

1. Introduction

Emissions from vehicles and power station using liquefied petroleum gas (LPG) contribute to the main source of harmful volatile organic compounds (VOC)s.[1,2] With escalating rigorous emission standards, effective catalytic oxidation of VOCs is increasingly important.[3,4] In comparison with Pt, Pd is known for its activity for many reactions including propane oxidation due to its resistance to poisoning by traces of CO,[5] and its tolerance to moisture.[6] However, the deactivation still constitutes a major challenge. In a recent study [7] of catalytic activity of Pd and Rh for CO and propane oxidation, the activity is shown to decrease at high temperature due to agglomeration of the nanoparticles as result of metal oxidation. In another study,[8] the low activity of propane oxidation over pure Pd/Al_2O_3 was ascribed to sintering and reducibility of the active site PdO_x and generation of metallic Pd^0. Bimetallic catalysts are considered a promising alternative in terms of stability and high activity in comparison with monometallic Pd.[9] In a study by Lang et al,[10] nanoporous AuPd showed higher catalytic activity and improved electrochemical stability toward methanol oxidation. Similarly, Co_3O_4-supported AuPd showed higher catalytic activity and better stability than supported Au and Pd for toluene oxidation due to a strong interaction between AuPd and the support.[11] Promotion of catalytic activity of pure noble metal such as Pt and Pd with lower low-cost transition metals, such as Ni, Cu, Co, etc. was found however, long-term durability is an issue, as degradation of PtCo cathode catalyst.[12] On the other hand, supports have been shown to exhibit significant effects on the catalytic activity of nanoparticles, including providing oxygen during propane oxidation (e.g., TiO_2 or CeO_2) [13] or assisting generation of active species.[14] Also, the acid/base strength of the support is shown to influence the catalytic performance in terms of dispersion and oxidation state of the supported Pd or Pt. In a study by Yoshida et al,[15] the effects of support (MgO, Al_2O_3, SiO_2- Al_2O_3) and additives on the catalytic activity of propane oxidation were investigated, showing that the catalyst performance is enhanced with more acidic support and with higher electronegativity of the additives. To increase the activity and stability, the alloying of Pd with Au has been considered an important approach since Au has a higher oxidation potential than Pd. While PdAu has been studied for many catalytic reactions,[16] to the best of our

knowledge, this study of AuPd nanoalloys for propane oxidation under different reaction conditions is the first example of its kind.

The understanding of the surface catalytic sites is important for the design of the bimetallic nanoalloys catalysts, for which in-situ diffuse reflectance infrared Fourier transform spectroscopy (DRIFTS) technique has proven to be powerful in probing the surface catalytic sites, as shown in our recent study of AuPd on different supports for CO oxidation.[17] While the as-synthesized AuPd nanoparticles were under very extensive tensile stress, the thermochemical treatment of the nanoparticles and the type of the support were shown to relieve a significant part of the tensile stress, leading to the random distribution of Au and Pd atoms in the nanoparticles. The formation of intermediate species during propane oxidation and their role in the reaction mechanism is a focal point in studies of Pt or Pd catalysts.[18] In a recent DRIFTS study of propane oxidation over Pt/Al_2O_3,[19] oxy-carbon species, such as acetate, enolate, aliphatic ester, and acetone were detected. It was found that an increasing concentration of oxy-carbon species had no effect on CO_2 production, indicating that these species are inert spectators during propane oxidation. The intermediate species grow on Pt/ Al_2O_3 surface and then spill over to the support Al_2O_3 surface. In another DRIFTS study by Faria et al,[20] of $Pd/ Al_2O_3/CeO_2$ for oxidative stream reforming of propane, it was shown that the formation of formate species ($HCOO^-$) is favored over $Pd/CeO_2/Al_2O_3$ while bicarbonate is detected over Pd/Al_2O_3.

While synergistic effects have been shown in previous experimental and theoretical studies of differently-prepared PdAu catalysts in other catalytic reactions, little has been known in terms of the roles of metal-support interaction, bimetallic composition and thermochemical processing in terms of the specific catalyts' phase structures and surface sites. Herein we describe novel findings of an in-situ DRIFTS study of PdAu nanoalloys with different bimetallic compositions and on different supports in propane oxidation, aiming at understanding the propane oxidation pathways and the catalytic activity in relation to the nanocatalyst's atomic-scale structure and surface-active sites. This understanding is aided by synchrotron X-ray diffraction (XRD) coupled to atomic pair distribution function (PDF) analysis for assessing the detailed nanoalloy's atomic-scale structures.

2. Experimental Section

Chemicals. Palladium (II) acetylacetonate ($Pd(acac)_2$, 97%), oleylamine ($CH_3(CH_2)_7CH=CH(CH_2)_8NH_2$, 70%), and borane-morpholine (95%) were purchased from Aldrich. Hydrogen tetrachloroaurate (III) hydrate ($HAuCl_4.xH_2O$, 99.9%) was purchased from Strem Chemicals. Other chemicals such as ethanol, hexane, and isopropanol were purchased from Fisher Scientific. Gases of propane (1 vol.% balanced by Ar), H_2 (99.99 vol.%), N_2 (99.99 vol.%) and O_2 (20 vol.% balanced by N_2) were obtained from Airgas. All chemicals were used as received. TiO_2 was purchased from Acros organics. $Al_2O_3$was purchased from Alfa Aesar.

Synthesis of PdAu nanoparticles. The synthesis of PdAu NPs involved the reduction reaction of two metal precursors.[21] Briefly, palladium (II) acetylacetonate and $HAuCl_4.xH_2O$ were dissolved in a desired molar ratio into 15.0 ml oleylamine in a glass vial by heated up to 40 ^oC with 1.9 mmol borane morpholine at 75 ^oC under N_2 atmosphere. The resulted solution was then heated up to 220 ^oC and kept for 30 minutes before cooling down to 70 °C. The NPs were first precipitated out by adding 40 mL isopropanol for centrifugation at 3000 rpm for 20 min and then re-dissolved in 15 mL hexane and 35 ml ethanol mixture cleaning solvent for centrifugation at 3000 rpm for 30 min. The NPs were redispersed in hexane solvent for further use.

Catalysts preparation. The catalysts were prepared from these as-synthesized nanoparticles, including assembling, and thermal activation. TiO_2, and Al_2O_3 powder were used as support materials which were mixed with controlled amount of as synthesized nanoparticles followed by sonication and overnight stirring. The product powder was collected and dried under N_2.

TiO_2, and Al_2O_3 -supported nanoparticles were activated by thermochemical processing, details of which were reported previously.[22] Typically, the supported nanoparticles were first treated at 120 ^oC under N_2 to remove the organic solvent. This was followed by heating at 260 °C under 20% O_2 (balanced by 80% N_2) for 1 hr to remove the organic capping molecules, and then to 400 °C under 15% H_2/85% N_2 for 2 hours for calcining the catalysts. The weight loading of the TiO_2 and Al_2O_3 supported PdAu catalysts were around

5% for most of the catalysts studied in this work, which were confirmed by ICP-OES analysis. For example, the metal loading of $Pd_{31}Au_{69}/Al_2O_3$ was 4.5 wt% whereas $Pd_{31}Au_{69}/TiO_2$ was 5.3 wt%.

Catalytic activity measurement. To measure the catalytic activity of supported PdAu catalysts for propane (1 vol.% balanced by Ar) + O_2 (20 vol.% balanced by N_2) reaction, a custom-built system was employed, including a temperature-controlled reactor, gas flow/mixing/injection controllers, and an on-line gas chromatograph (Shimadzu GC 8A) equipped with 5A molecular sieve, Porapak Q packed columns, and a thermal conductivity detector. The catalysts were loaded in a quartz micro-reactor tube (inner diameter: 4 mm) and wrapped by quartz wool in the middle of the tube (length of the catalyst bed: 6 mm). At a flow rate of 20 ml/min, the system was injected with the feeding gas (0.8 vol.% propane +10 vol.% O_2 balanced by N_2) through the mounted catalyst in the quartz micro reactor. The residence time was about 0.2 seconds. Gas hourly space velocity (GHSV) in the system is around 16000 h^{-1}. Temperature control was achieved by a furnace coupled with a temperature controller. The performance of the catalysts of propane oxidation were determined by analysis of composition of the tail gas effusing from the quartz micro reactor packed with the catalyst fixed bed by the on-line gas chromatograph.

Morphology and Composition Characterization. Transmission Electron Microscope (TEM) was used to determine the size of nanoparticle. The nanoparticle samples were suspended in hexane solution and were drop cast onto a carbon-coated copper grid followed by solvent evaporation in ambient atmosphere at room temperature.

High-Angle Annular Dark-Field Scanning (HAADF-STEM)-Energy Dispersive spectroscopy (EDS) was utilized to determine the morphology and map the elemental distribution of the nanoparticles. Following suspension of the sample in hexane solution, then the nanoparticles were drop cast onto carbon-coated copper grid. The measurements were performed on JEOL-ARM200F instrument with an acceleration voltage of 200 kV

Inductively Coupled Plasma - Optical Emission Spectroscopy (ICP-OES). ICP-OES was employed to examine the nanoparticle composition. It was done on a Perkin Elmer 2000 DV ICP-OES instrument using a cross flow nebulizer with the following parameters: plasma 18.0 L $Ar_{(g)}$/min; auxiliary 0.3 L

$Ar_{(g)}$/min; nebulizer 0.73 L $Ar_{(g)}$/min; power 1500 W; peristaltic pump rate 1.40 mL/min. Elements <1.0 mg/L were analyzed using a Meinhardt nebulizer attached to a cyclonic spray chamber to rise analyte sensitivity with the following parameters: 18.0 L $Ar_{(g)}$/min; auxiliary 0.3 L $Ar_{(g)}$/min; nebulizer 0.63 L $Ar_{(g)}$/min; power 1500 W; peristaltic pump rate 1.00 mL/min.

Ex situ HE-XRD measurements were carried out both on in house equipment and using synchrotron radiation x-rays (E= 80.725 keV) at the beamline 1-ID at the Advanced Photon Source at the Argonne National Laboratory.

The XRD diffraction data were reduced to the so-called structure factors, *S(q)*, and then Fourier transformed to atomic PDFs *G(r)*, using the relationship $G(r) = \frac{2}{\pi}\int_{q=0}^{q_{max}} q[S(q)-1]\sin(qr)dq$, where q_{max}= 25 $Å^{-1}$ in the present experiments. The wave vector q is defined as $q=4\pi\sin(\theta)/\lambda$, where θ is half of the scattering angle and λ is the wavelength of the x-rays used. Note, as derived, atomic PDFs G(r) are experimental quantities that oscillate around zero and show positive peaks at real space distances r, where the local atomic density ρ(r) exceeds the average one ρ_o. This behavior can be expressed by the equation $G(r) = 4\pi r\rho_o[\rho(r)/\rho_o-1]$, which is the formal definition of the PDF G(r). High-energy XRD and atomic PDFs have already proven to be very efficient in studying the atomic-scale structure of nanosized materials.[23,24]

Diffuse Reflectance Infrared Fourier Transform Spectroscopy (DRIFTS). DRIFTS measurements were performed under propane oxidation reaction conditions was on a Bruker Vertex 70 FTIR spectrometer with a MCT detector and a Praying MantisTM Diffuse Reflectance Accessory (Harrick Scientific Products, Inc.). Briefly, the sample cup in Praying MantisTM Diffuse Reflectance Accessory was filled up with 30 mg of $PdAu/Al_2O_3$ catalysts for the propane oxidation reaction at 350 ºC. In-situ DRIFTS spectra were obtained with A Bruker Vertex 70 FTIR spectrometer equipped with a MCT detector and a Praying Mantis™ Diffuse Reflectance Accessory (Harrick Scientific Products, Inc.) using liquid nitrogen to cool down the MCT detector. The DRIFT measurements were taken at 64 scans with resolution of 2 cm^{-1}.

Computational Modeling. Ab-initio calculations were conducted by density functional theory (DFT) utilizing DMol[3] program coming as a part of Materials Studio program. In the computation, the generalized gradient approximation (GGA) were used. Minimization of energy of all model atomic configuration for unsupported PdAu were carried out. To interrogate the interaction between propane, oxygen, intermediate species and the model atomic configurations, the energy of adsorption of propane on the model atomic configurations was measured. It was calculated by $E_{\text{ads}} = -(E_{\text{propane-metal}} - E_{\text{metal}} - E_{\text{propane}})$, where, $E_{O_2-\text{metal}}$, E_{metal} and E_{propane} are total energy for the propane-metal complex, the isolated metal configuration, and the isolated propane molecule, respectively.

3. Results and Discussion

In this section, results from the morphological and structural characterizations of PdAu nanoparticles are first described to demonstrate the composition controllability and phase structures of the bimetallic nanoparticles. Secondly, the catalytic activities of propane oxidation over the catalysts are discussed in terms of their dependencies on the bimetallic composition and the thermochemical treatment parameters. Finally, the catalytic synergy in correlation with bimetallic composition and alloying structure is discussed.

3.1 Morphology, composition and phase structures

The composition of the PdAu nanoparticles was analyzed using ICP-OES, which revealed a linear relationship between the Au% in the nanoparticles and the Au% in the feeding composition in the synthesis solution (Fig.S1A, ESI†), demonstrating an excellent controllability of the bimetallic composition in the synthesis. There is a slight lower Au% in the NPs than in the synthesis feeding, indicating that Pd is slightly more favorable in the bimetallic nanoparticles than Au. A set of samples, $Pd_{91}Au_9$, $Pd_{55}Au_{45}$, and $Pd_{31}Au_{69}$ NPs[17], were examined in this study, which features an average size of 6.5 ±0.6 nm, 5.5±0.8 nm and 5.3±0.9 nm, respectively (Fig. S1B, ESI†). The NPs were supported on TiO_2; and were thermochemically treated to activate the catalysts, yielding an average size of 6.5 nm for all NPs on the support [25]. The morphology and elemental distribution were determined using HAADF-STEM coupled with EDS mapping analysis.

Based on the EDS mapping data for $Pd_{55}Au_{45}/TiO_2$ sample (Fig. S1C, ESI†), the distribution of the two metals in the bimetallic NPs is characteristic of a random alloy.

A representative set of X-ray powder diffraction (XRD) pattern for the $PdAu/Al_2O_3$ NPs is shown in Fig. 1, featuring a face-centered cubic structure. The diffraction peaks located between corresponding Au and Pd peaks, indicating of formation of alloy structure. The diffraction peak at 38.2º corresponding to Au (111) shifts to higher diffraction position as Au% decreases, an indication of interatomic distance shortening. For $Pd_{55}Au_{45}$ nanoparticles, the Bragg peaks are very broad, indicating low crystallinity. The diffraction peaks at 44.3º and 64.5º were assigned to Au (200) and Au (220), respectively. The spectra did not display the signature of oxygen species assigned to PdO at 2θ of 33.5º.[26] This was further confirmed by XPS analysis of the nanoalloys (see Fig. S2, ESI†). The detected peak positions for Pd $3d_{3/2}$ and $3d_{5/2}$ (~340.2 eV and ~335 eV) were characteristic of Pd(0) state, and no oxygen species (at 343 eV) were detected[26]. Note that the XRD data were collected after the catalysts were treated at 260 °C / O_2 followed by 400 °C /H_2 treatment, in which PdO could be reduced to Pd^0.

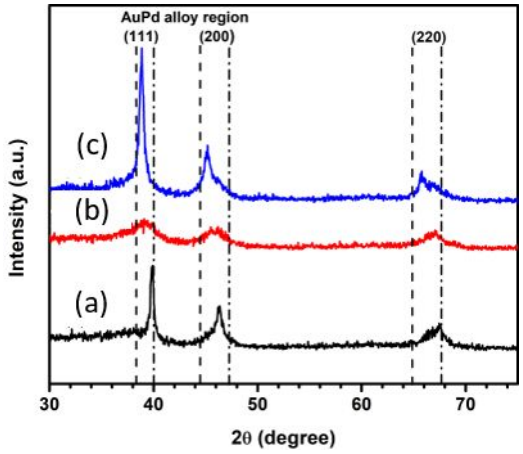

Fig 1. XRD patterns of NPs (a) $Pd_{91}Au_9/ Al_2O_3$, (b) $Pd_{55}Au_{45} / Al_2O_3$, (c) $Pd_{31}Au_{69}/ Al_2O_3$ **(**Note that the size of Al_2O_3 are too fine to display diffraction peaks)

The technique of HE-XRD coupled with PDF was used to examine the atomic-scale alloying phase structure. Fig. 2A displays a set of PDFs for PdAu NPs supported on Al_2O_3 after thermochemical treatment. The arrangement of sharp peaks in the atomic PDFs represents presence of a well-defined atomic

coordination spheres in PdAu /Al_2O_3 NPs. The experimental PDFs fits well with the face-centered cubic (fcc) structure model, from which the interatomic distances could be approximated based on lattice parameter. Lattice parameters of PdAu NPs supported on Al_2O_3 and TiO_2 were extracted from the experimental PDF data, which are shown in Fig. 3B. For PdAu/TiO_2, the lattice parameter increases with increasing Au% in an approximately linear fashion with a slope approaching that predicted by Vegard's law. However, the situation is different for PdAu/Al_2O_3, which showed a slope smaller than that according to Vegard's law. This finding suggests that the Al_2O_3 supported PdAu nanoparticles were under very compressive stress.[27] This phenomenon in nanoparticle is due to modification of electronic property of the alloy. However, the type of the support appears to relieve a significant part of the compressive stress due to the nature of interaction between nanoparticle and support.[17] In comparison with bulk Au (4.079 Å) and bulk Pd (3.891 Å), lattice shrinking has been reported for nanoparticle counterparts on different supports, including Au on TiO_2 (3.786 Å), Pd on TiO_2 (3.785Å),[28] Au on Al_2O_3 (4.068 Å), and Pd on Al_2O_3 (3.88 Å).[26] Note that for carbon support, lattice expansions were observed, e.g., Au_9Pd_{91}/C (3.941 Å), $Au_{45}Pd_{55}$ (3.982 Å), $Au_{69}Pd_{31}$ (4.015 Å),[17] and Pd/C (3.89 Å) and AuPd/C (3.93 Å).[29] These subtle differences indicate that the lattice strain characteristics of the nanoparticles are highly dependent on the nanoparticle-support interactions.

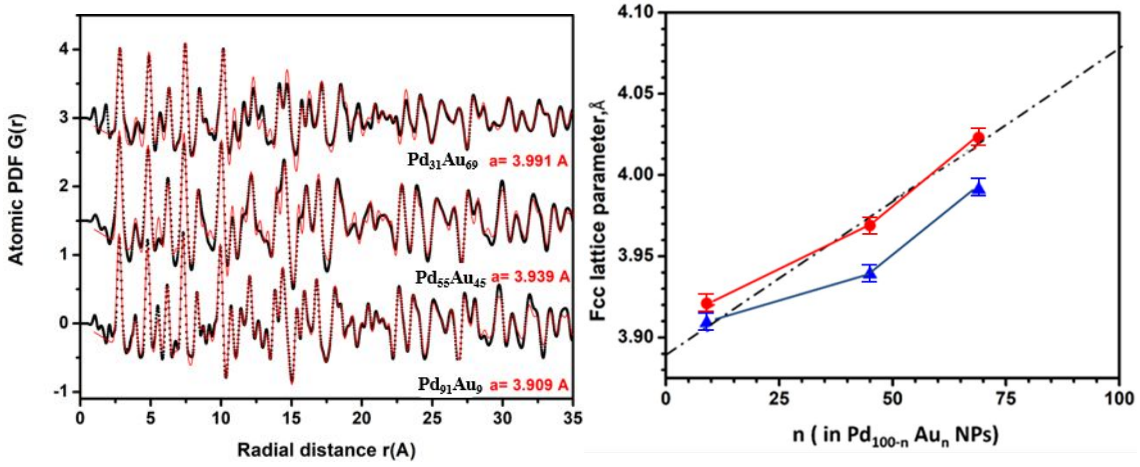

(A) (B)

Fig. 2 Experimental (symbols in black) and model (line in red) total atomic PDFs for PdAu /Al_2O_3 (A), and Plots of fcc-lattice parameter of PdAu /Al_2O_3 NPs (symbols in blue) and AuPd/TiO_2 (symbols in red) (B), as a function of the relative Au content in the NPs. Broken (dash dot) line represents a 1:1 relationship.

The overall lattice shrinking for $PdAu/Al_2O_3$ in comparison with $PdAu/TiO_2$ is believed to reflect the difference of metal adhesion on the two different supports. Theoretical studies [30] and experimental data [31] showed that the metal-support interaction strongly depends on the chemical nature of the metal and the support, especially the oxophilicity.[32] The adhesion energy of Pd/Al_2O_3 (4.38 J/m^2) and Au/Al_2O_3 (2.31 J/m^2) have been shown to be higher than those for Pd/TiO_2 (1.092 J/m^2) and Au/TiO_2 (0.292 J/m^2) [33-34], which suggests a stronger metal-support interaction for $PdAu/Al_2O_3$ than for $PdAu/TiO_2$. The stronger interaction could lead to a smaller contact angle of NP on the support, under which lattice shrinking could occur. For $PdAu/Al_2O_3$ with Au% > 40%, the lattice parameter approaches to that for Pd. In comparison, the lattice parameter of $PdAu/TiO_2$ approached Vegard's law, indicating a better degree of alloying. The strong interaction between PdAu NPs and Al_2O_3 lead to a partial segregation of $Pd_{55}Au_{45}$ and $Pd_{31}Au_{69}$ (Fig.2b). Another factor affecting the metal segregation is the difference of surface energy,[35], e.g., Pd's surface energy is 2.04 J/m^2 whereas Au's surface energy is 1.62 J/m^2, which could lead to surface enrichment of Au whereas the nanoparticle core is enriched with Pd. Indeed, EDS mapping data showed that Au atoms in $Pd_{91}Au_9$ tend to segregate toward the NP surface.[17] Moreover, the strong metal - oxide support could also be lowering sintering rate of NPs, which is important for maintaining the high catalytic activity.[36]

3.2 Catalytic oxidation of propane

3.2.1. Catalytic activity. In contrast to the CO oxidation reaction, which is generally believed to follow a Langmuir-Hinshelwood mechanism, i.e., both CO and O_2 are activated by co-adsorption, the propane oxidation involves the chemisorbed and activated O species reacting with poor adsorption of propane . Since the oxygen activation is essential in the catalytic oxidation, the determination of propane oxidation intermediate species provides information for assessing the surface sites on the nanoalloy catalysts.

The measurement of the catalytic activity for propane oxidation focused on PdAu NPs of different compositions supported on TiO_2 and Al_2O_3 supports. Fig 3 shows a representative set of catalytic data for the as-prepared catalysts (260 °C /O_2 treatment followed by 400 °C /H_2 treatment) and the re-oxidized catalysts (260 °C /O_2-treatment of the as-prepared catalysts). First, the catalytic activity depends on the

bimetallic composition and the chemical nature of the support, exhibiting the order of $Pd_{55}Au_{45}$ > $Pd_{91}Au_9$ > $Pd_{31}Au_{69}$, for both TiO_2 and Al_2O_3 supported catalysts (Fig. 3A-B). Secondly, the overall catalytic activity was found to be almost independent on the O_2 treatment (260 °C /O_2) for most of the catalysts, except for $Pd_{91}Au_9/Al_2O_3$ which showed a subtle increase after the O_2 treatment. This finding in contrast to data for Pd alloyed with base transition metals where oxophilicity has strong impact on catalytic activity.[37] Note that the catalytic data of commercial Au/TiO_2 shows very low activity in comparison to binary PdAu catalyst (see Fig S5A, ESI†). The $PdAu/TiO_2$ catalysts show clearly an enhanced catalytic activity, e.g., $Pd_{55}Au_{45}/TiO_2$ which has values of T_{10} = 190 °C and T_{50} = 220 °C (see Fig. 4A-B) in comparison with values of T_{10} = 290 °C and T_{50} = 350 °C previously reported for 2 wt% Pd/TiO_2.[38] For $Pd_{55}Au_{45}/Al_2O_3$, an enhanced activity was also observed, but the catalytic activities in comparison with Pd/Al_2O_3 depends on the preparation methods for the catalysts. Examples of the activities reported for Pd/Al_2O_3 include T_{10} = 320 °C and T_{50} = 390 °C,[39] and T_{10} = 240 °C and T_{50} = 320 °C .[40] For a commercial 5 wt % Pd/Al_2O_3, T_{10} = 225 °C and T_{50} = 290 °C (see Fig.S5B, ESI†). Again, the comparison was limited at this point because it was affected by the differences in particle sizes and catalyst preparation methods.

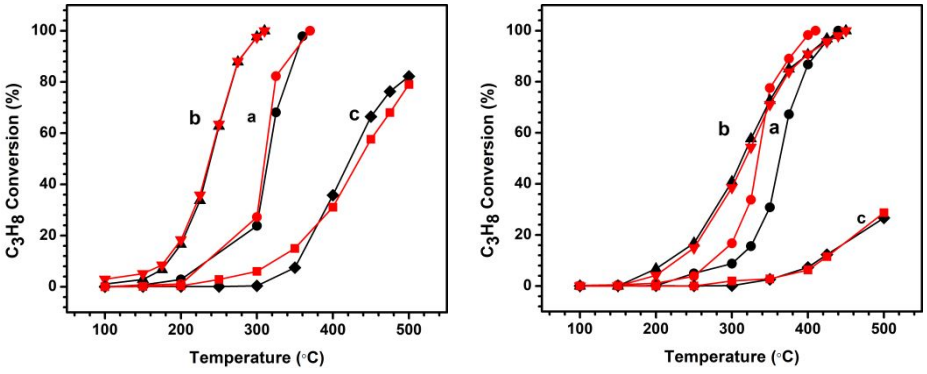

Fig. 3 Comparisons of propane conversion activities over PdAu NPs supported on two different supports: (A) TiO_2 and (B) Al_2O_3. $Pd_{91}Au_9$ (a, circle); $Pd_{55}Au_{45}$ (b, triangle); and $Pd_{31}Au_{69}$ (c, square). Catalyst treatments: (1) as-prepared catalysts (260 °C / O_2 treatment followed by 400 °C /H_2 treatment, black), 2) 260 °C/ O_2 re-treated catalysts (red).

By comparison of the catalytic activities in terms of the oxidation temperatures (Fig. 3), a maximum catalytic activity is revealed for the catalysts with a Pd:Au ratio of 1:1. Interestingly, a close examination of the data in Fig. 3 indicates subtle differences in terms of the relative T_{10}, T_{50} and T_{75} values for the

catalysts before and after the oxidative thermochemical treatment for Pd_nAu_{100-n} /TiO_2 (I) and over Pd_{100-n} Au_n/Al_2O_3 (II) (Fig. 4). Note that for $Pd_{31}Au_{69}/Al_2O_3$ (II) both T_{50} and T_{75} fall above the temperature range because of its low activity. For $Pd_{100-n}Au_n/TiO_2$ (I), while there were small changes in most the cases for <50%Au or > 50%Au, little change was observed for ~50%Au before and after the oxidative thermochemical treatment. Similar results were also obtained for Pd_{100-n} Au_n/Al_2O_3 (II) with <50%Au and ~50%Au. These observations are remarkable, suggesting not only the operation of a composition-dependent catalytic synergy, especially for the PdAu NPs with ~50% Au. Note that the present work focused on studying the bimetallic composition-activity dependence of the supported PdAu nanoparticles in the propane reaction in terms of intermediates in relation with catalytic activity. There is a need to dunderstan the stability and it would involve testing the catalysts in different gas mixtures and temperatures or different ageing conditions. There is also a need to compare the stabilities of AuPd and Pd catalysts. Our preliminary work under a very limited condition showed an indication of higher activity and stability for a certain AuPd catalyst, but the confirmation, especially in comparison with Pd catalysts under the same or comparable particle sizes and by similar preparation methods, will be needed in the future work.

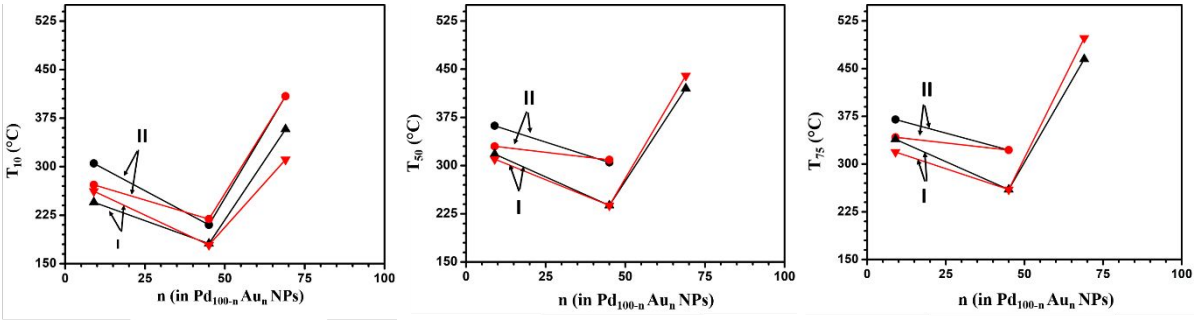

(A) (B) (C)

Fig. 4 Plots of T_{10} (A), T_{50} (B), and T_{75} (C) values vs. bimetallic composition for propane oxidation over Pd_{100-n} Au_n /TiO_2 (I, triangles); and over Pd_{100-n} Au_n /Al_2O_3 (II, circles) catalysts for the fresh catalysts (black) and the treated under O_2 at 260 °C for 30 min (red).

In order to understand the mechanistic details, the kinetic data was examined, revealing two different E_a values for low and high reaction temperature ranges (see Fig. S3, ESI†). The overall E_a value is higher in the low temperature range (100 to 270 °C) than that in the high temperature range (300 to 500°C). Secondly, E_a exhibits a minimum at an Pd:Au ratio of ~50: 50 , consistent with the reaction temperature

data. The overall E_a values in the low temperature range for the catalysts are slightly lower than those reported for catalytic oxidation of propane (60 - 90 kJ/mol).[1] In addition to the dependence of E_a on the bimetallic composition, a clear dependence on the thermal treatment condition was also revealed. In the low temperature range (Fig. S4A, ESI†), the activation energy was increased after O_2 treatment for Pd_nAu_{100-n} /TiO_2 with n < 50. This is consistent with measured T_{10} values. (see Fig. 4A). However, the activation energy for n< 50 dropped in case of Al_2O_3 supported Pd_nAu_{100-n} (see Fig. S4C, ESI†). For n greater than 50 (e.g., $Pd_{31}Au_{69}$ /TiO_2), the activation energy showed a decrease after O_2 treatment. This is also consistent with T_{10} values (see Fig. 4A). Note that the activation energy remained unchanged after O_2 treatment for n~50 which is consistent with measured T_{50} values (see Fig. 4B). In the high temperature range (Fig. S4B and S4D, ESI†), the activation energy showed an increase for n<50 and an increase for n> 50 after O_2 treatment, which are consistent with the trend of T_{75} values (see Fig. 4C).

Taken together, the kinetic results suggest a switching-type catalytic activities in terms of lower and higher T_{10} and T_{75} values in the low and high reaction temperature range, as shown in Fig. 4A and 4C, in terms of the oxidative treatment. The fact that the increase of E_a for the oxidized Pd_nAu_{100-n}/TiO_2 catalysts for n< 50 did not change the conversion activity is indicative of the immunity of both Au and Pd from oxidation in the nanoalloy under the reaction condition. The finding that PdAu/TiO_2 exhibits an activity higher than that for PdAu/Al_2O_3 is believed to reflect to a combination of the higher degree of alloying in the NPs and the higher oxygen capability for TiO_2. For PdAu/Al_2O_3, in which the compressive stress is at maximum (Fig. 2B), a down shift of d-band level with respect to Fermi level[41] could reduce the binding energy of propane or intermediate species and enhance the oxidation.

3.2.2 In-situ DRIFTS characterization

TiO_2 is known for providing activation of lattice oxygen, [42] leading to a high oxygen capacity. PdAu/Al_2O_3, while showing an activity lower than PdAu/TiO_2, exhibited a composition dependence of activity similar to PdAu/TiO_2. There is also a significant lattice shrinking for Au% > 40% in comparison with the fully-alloyed character of PdAu/TiO_2. In this work, Al_2O_3 support was used as an example for

studying the catalytic synergy of AuPd NPs in propane oxidation. In comparison with TiO_2, Al_2O_3 is known for its strong interaction with noble metals and exhibition of high resistance for nanoparticle aggregation especially at high reaction temperature which is required for oxidation of hydrocarbons such as propane. [43] Based on these observations, an in-situ DRIFTs study was performed for propane oxidation over $PdAu/Al_2O_3$ catalysts in an attempt to develop the correlation among the nanostructure, the activity, and the surface species. Surface species over $PdAu /Al_2O_3$ catalysts were monitored by DRIFTS during propane oxidation at 350 ºC under the flow rate of 80 mL/mins with O_2/C_3H_8 ratio at 5:1. Fig. 5 represents a typical set of DRIFTS spectra monitoring the surface species during propane oxidation over different composition of $PdAu /Al_2O_3$. The observed peaks depend on the bimetallic composition in terms of peak position and intensity. As the reaction progresses, the intensities of the bands become stronger in case of $Pd_{91}Au_9$ (Fig. 5A) and in $Pd_{55}Au_{45}$ (Fig. 5B). However, the peak intensity is much weaker for $Pd_{31}Au_{69}$ (Fig. 5C). The peak at ~2970 cm^{-1} is assigned to alkane C-H vibration bonds of gaseous propane, while bands around 2902 cm^{-1} attributed to CH_2(ads) and CH_3 (ads) species.[20] The band observed in the range ~ 2340-2360 cm^{-1} are characteristic for gaseous CO_2.[44] Note that the spectra did not display the signature of adsorbed CO species in the range of around (2200 to 2400 cm^{-1}).[45] Major peaks in the range of ~ 1730 – 1330 cm^{-1} were clearly detected over $Pd_{55}Au_{45}$ and $Pd_{91}Au_9$, part of which were weak but observable over $Pd_{31}Au_{69}$. Note that the catalytic activity measurement was taken in a packed quartz reactor, whereas the DRIFTs cell was an open reactor. The difference in the experimental set-ups could result in different gas composition, flow rate and GHSV between these two measurements, but our analysis of the DRIFTS data in this work mainly focused on the identification of the surface species, rather than a detailed correlation with their reaction kinetics.

The evolution of oxy-carbon bands are examined in detail in the range of 1730-1330 cm^{-1} (Fig. 5 right panel). Detailed peak assignments are shown in Table S1, ESI†. The peaks detected at 1560 and 1455 cm^{-1} (Fig. 5A right) and 1580, 1460 cm^{-1} (Fig. 5B right) are assigned to adsorbed acetate species.[46,47] The band at 1683 cm^{-1} is (Fig. 5A right) and 1681 cm^{-1} (Fig. 5B right) are assigned to adsorbed acetone species.[48] The shoulder band at 1730 -1733cm^{-1} (Fig. 5A, B) are assigned to adsorbed carbonyl group with aliphatic ester group.[49,50] The band at 1645 cm^{-1} is assigned to adsorbed bicarbonate species (Fig. 5A, B)

.[51,52] The band at 1593 cm^{-1} is consistent with absorption of formate species (Fig. 5A).[53,54] The peak at 1470 cm^{-1} (Fig. 5A) is attributed to adsorbed methoxy groups.[55,56]

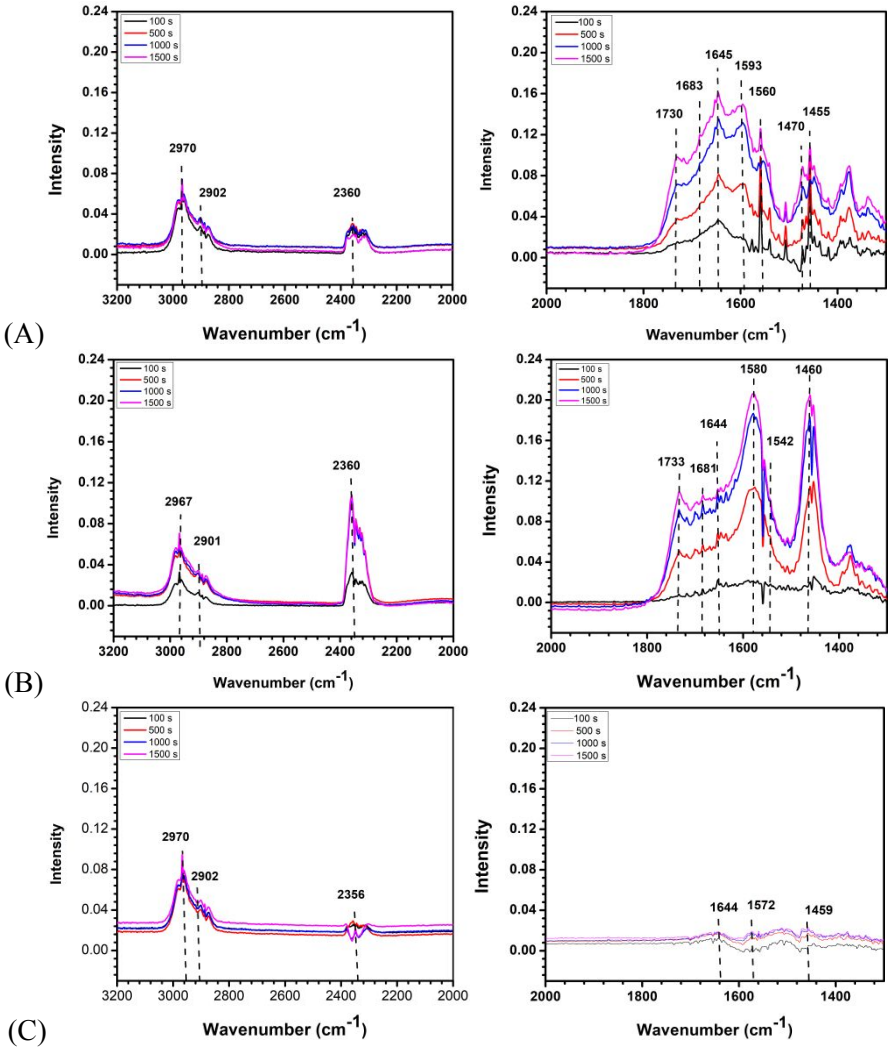

Fig. 5 In-situ DRIFTS spectra recorded during propane oxidation over $Pd_{91}Au_9/Al_2O_3$(A); $Pd_{55}Au_{45}/Al_2O_3$ (B); and $Pd_{31}Au_{69}/Al_2O_3$ (C) at 350 °C; The spectra in the right are zoomed views of the spectra in the 1730 to1330 cm^{-1} region.

Propane oxidation over a commercial Pd/Al_2O_3 catalyst was also examined by in-situ DIRFTs to probe the surface species during propane oxidation. The reaction temperature was slightly different. Fig. S6, ESI†, shows a representative set of DRIFTS spectra. As shown in (Fig. S6, ESI†), there are four major peaks observed for Pd/Al_2O_3. The peaks at 1585 and 1470 cm^{-1} are characteristic of adsorbed acetate species. The band at 1675 cm^{-1} is assigned to adsorption of acetone. The shoulder band at 1730 cm^{-1} is

assigned to carbonyl group with aliphatic ester group. In comparison with PdAu, the peaks of acetate over Pd/Al_2O_3 were detected at higher wavenumber and they were observable over $Pd_{55}Au_{45}/Al_2O_3$ and $Pd_{91}Au_9/Al_2O_3$ only. The peaks of acetone species were found for $Pd_{91}Au_9/Al_2O_3$ and $Pd_{55}Au_{45}/Al_2O_3$ only. Similarly, the peaks for the aliphatic ester were only observable for $Pd_{55}Au_{45}/Al_2O_3$ and $Pd_{91}Au_9/Al_2O_3$.

It is evident that oxy-carbon species (COO, OCO, CCO, etc.) were observed on these catalysts during the propane oxidation reaction. The subtle differences in terms of the changes in peak intensities for the catalysts with different bimetallic compositions are further analyzed to assess the formation of different intermediate species during the oxidation reaction. Fig. 6A-B show the transient plots of peak intensities for several diagnostic bands, including aliphatic ester υ ($CH_3C(=O)$-O) ~ 1730 cm^{-1}, acetone υ ($(CH_3)_2C=O$) ~1681 cm^{-1}, bicarbonate υ_{as} ($HOCO_2^-$) ~1644 cm^{-1}, formate υ_{as} ($HCOO^-$) ~ 1593 cm^{-1}, acetate $\upsilon_{as}(CH_3CO_2^-)$ ~ 1560 cm^{-1}, displaying subtle differences. There is a clear increase of the oxy-carbon species as the reaction progresses for $Pd_{91}Au_9/Al_2O_3$ and $Pd_{55}Au_{45}/Al_2O_3$ while the change is insignificant in the case of $Pd_{31}Au_{69}/Al_2O_3$. (see Fig. S7, ESI†). Interestingly, for $Pd_{55}Au_{45}/Al_2O_3$ the growth rate of peak intensity for the adsorbed acetate species ($\upsilon_{as}(CH_3CO_2^-)$ ~1560 cm^{-1}) is much greater than those for the adsorbed aliphatic ester, acetone and bicarbonate species. For $Pd_{91}Au_9/Al_2O_3$, the growth rate for bicarbonate and formate species are slightly greater than the acetate, acetone, and ester species.

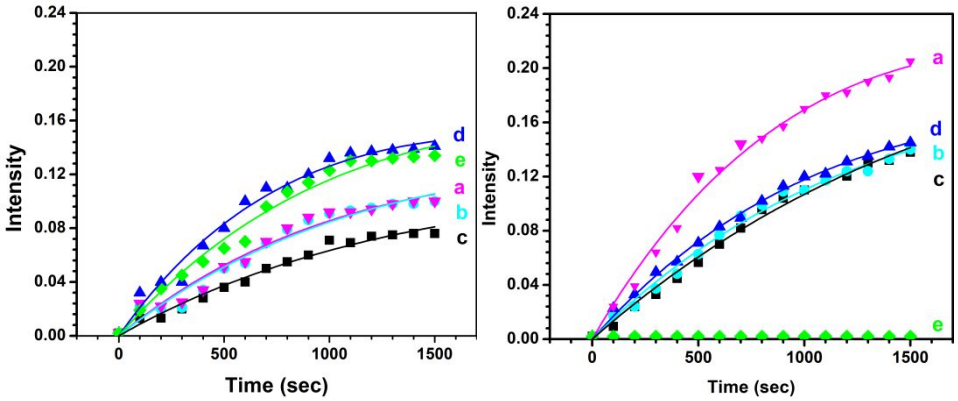

Fig. 6 (A-B) Plots of peak intensity (peak height) vs time for propane oxidation adsorption at 350 ºC for several major bands detected, including acetate $\upsilon_{as}(CH_3CO_2^-)$ ~ 1560 cm^{-1}(a, pink), acetone $\nu(CH_3)_2C=O$) ~1681 cm^{-1}(b,cyan), aliphatic ester υ ($CH_3C(=O)$-O) ~ 1730 cm^{-1} (c, black), bicarbonate υ_{as} ($HOCO_2^-$) ~1644 cm^{-1}(d, blue), formate υ_{as} ($HCOO^-$) ~1593 cm^{-1}(e, green), for $Pd_{91}Au_9/Al_2O_3$(A), and $Pd_{55}Au_{45}/Al_2O_3$ (B); for The data are extracted from Figure 6. The fitting curve was based on equation 1. See Table S4 for for claculated k_1 and k_2.

If first-order reactions are considered for adsoprtion and desorption of the intermediate species, i.e.,

$$R \overset{k_1}{\rightarrow} I_{ads} \overset{k_2}{\rightarrow} P \quad (1)$$

we would have the following type of equation for the surface corverage (θ: coverage of intermediate species, I_{ads}) vs. time:

$$\theta = (\frac{k_1}{k_1 - k_2}))(\exp(k_2 t) - \exp(-k_1 t)) \quad (2)$$

By appling the above equation to the data in Fig. 6 in terms of peak intensity, we obtain the values of the apparent rate constant (k_1 and k_2) (see Table S2). In general, the apparent rate constant is higher for the species showing a higher intensity (e.g., acetate 2.71×10^{-4}, $Pd_{55}Au_{45}$) than those with lower intensity (e.g., ester 1.38×10^{-4}, $Pd_{55}Au_{45}$). Interestingly, k_2 (e.g., bicarbonate 9.61×10^{-4}, $Pd_{91}Au_9$) is higher than k_1 (e.g., bicarbonate 2.22×10^{-4}, $Pd_{91}Au_9$) for all the intermediate species detected. The subtle differences of the apparent rate constants among the catalysts with different compositions are believed to reflect that the formation, desorption or further oxidation of intermediate species depend strongly on the surfcae active sites.

Fig. 7 compares the peak intensities for the oxy-carbon species identified in the range of 1730-1330 cm^{-1} for $Pd_{91}Au_9/Al_2O_3$, $Pd_{55}Au_{45}/Al_2O_3$, and $Pd_{31}Au_{69}/Al_2O_3$. It is clear that the acetate species is maximized over $Pd_{55}Au_{45}/Al_2O_3$ whereas the bicarbonate species is maximized over $Pd_{91}Au_9/Al_2O_3$. Between $Pd_{91}Au_9/Al_2O_3$ and $Pd_{55}Au_{45}/Al_2O_3$, a key difference is that while the growth rate for acetate species is greater for $Pd_{55}Au_{45}/Al_2O_3$, the growth rate for bicarbonate and formate species is greater for $Pd_{91}Au_9/Al_2O_3$, the latter of which also showed the extra ester species. This finding demonstrates that the chemical or intermediate species are strongly dependent of the bimetallic composition. For $Pd_{31}Au_{69}/Al_2O_3$, the peak intensities are much smaller than those for the $Pd_{91}Au_9/Al_2O_3$ and $Pd_{55}Au_{45}/Al_2O_3$.

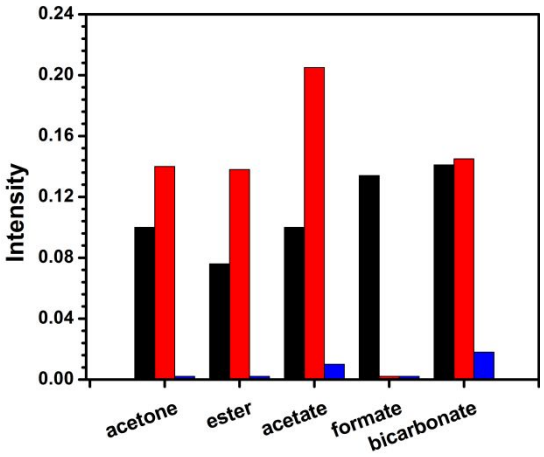

Fig. 7 Comparison of the DRIFTS peak intensities for some of the major intermediate species detected in propane oxidation at 350 ºC over $Pd_{91}Au_9/Al_2O_3$(black bars), $Pd_{55}Au_{45}/Al_2O_3$ (red bars), and $Pd_{31}Au_{69}/Al_2O_3$ (blue bars) catalysts. The intermediate species are arranged from non or 1st C-C bond cleaved oxidation species (acetone, ester, and acetate) to complete C-C bond cleaved oxidation species (formate, and bicarbonate).

In Fig. 7, the DRIFTS peak intensities of the major intermediate species detected in propane oxidation at 350 ºC over the PdAu of three different compositions catalysts intermediate species are arranged from non or 1st C-C bond cleaved oxidation species (acetone, ester, and acetate, i.e., Group-I) to 1st and 2nd C-C bond cleaved oxidation species (formate, bicarbonate, i.e., Group-II). In comparison with the experimentally-observed maximum activity for the catalyst with Pd:Au~50 (see Fig. 4A, B) for propane oxidation, the catalyst composition dependence of the detected intensities for Group I species seem to correlate well in terms of the relative amount of surface species. For Group-II species, in comparison with the relatively high levels of surface species associated well for $Pd_{91}Au_9/Al_2O_3$. The absence of formate species and the reduced level of bicarbonate species for propane oxidation of $Pd_{55}Au_{45}$ are evident, suggesting an effective conversion of Group-II species to CO_2. There exist different possibilities for the absence of formate species. By comparing the results for PdAu catalysts with different compositions, we were able to assess the possibilities of different reaction pathways, but our assessments were largely linked to the dependences of Group I or II species on the bimetallic composition. In other words, this result correlates in a certain degree with the higher catalytic activity $Pd_{55}Au_{45}$. Since there is essentially no or very low activity for the Au-rich catalyst ($Pd_{31}Au_{69}$), the detected Group-I and -II species are essentially zero or very small

3.3. Catalytic synergy in terms of composition-structure-activity correlation

The results shown in Fig. 7 provided the relative abundances of the peaks associated with the chemical and intermediate species being detected for us to assess relative amounts of the non or 1st C-C bond cleaved oxidation species (acetone, ester, and acetate, i.e., Group-I) to 1st and 2nd C-C bond cleaved oxidation species (formate, bicarbonate, i.e., Group-II). For pure Pd and Pd-rich $Pd_{91}Au_9$, while the activity for C-H and first C-C bond cleavages is comparable to that for $Pd_{55}Au_{45}$, the cleavage of the second C-C bonds appears to be less effective (see Scheme 1). Therefore, there is a synergy for the catalytic activity of propane oxidation over $Pd_{55}Au_{45}$, showing activity enhancement by the introduction of an appropriate level of Au into the Pd alloy.

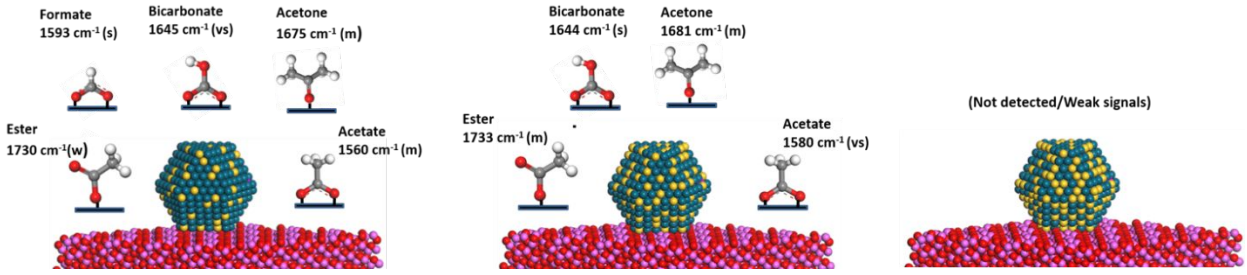

(A) (B) (C)

Scheme 1 Illustrations of the major intermediate species detected for propane oxidation over $Pd_{91}Au_9/Al_2O_3$ (A); $Pd_{55}Au_{45}/Al_2O_3$ (B); and $Pd_{31}Au_{69}/Al_2O_3$ (C). Atomic color codes: Pd (green), Au (yellow), C (gray), H (white), O (red)), and Al (pink). (vs, very strong; s, strong; m, medium; w, weak; vw, very weak)

In contrast to the absence of almost no intermediate species detected on Au-rich alloy (i.e., $Pd_{31}Au_{69}/Al_2O_3$), formate and biocarnoate were detected on Pd-rich and Pd~50% alloys (i.e., $Pd_{91}Au_9/Al_2O_3$ and $Pd_{55}Au_{45}/Al_2O_3$), which consistent with the high catalytic activities for both catalysts. However, in comparison with $Pd_{91}Au_9/Al_2O_3$, formate was not detected and the intensity of bicarbonate species was reduced for propane oxidation over $Pd_{55}Au_{45}/Al_2O_3$, indicating that the complete C-C cleaved products were likely released as CO_2. This finding is consistent with the higher activity of $Pd_{55}Au_{45}/Al_2O_3$ than $Pd_{91}Au_9/Al_2O_3$ (see activity data in Fig. 4). Since the propensity of oxidation of Au is much lower, the surface oxophilicity of $Pd_{91}Au_9/Al_2O_3$ is likely to be higher than $Pd_{55}Au_{45}/Al_2O_3$, which explains the difference in terms of retaining the adsorbed intermediate formate and bicarnoate species between the two catalysts. This difference in oxophilicity is also manifested by the lattice difference between these two

catalysts, i.e., the less oxophilic PdAu/Al_2O_3 showed a more significant lattice shrinking (see Fig. 2). The general correlation of oxophilicity to the lattice shrinking has been established in our previous studies [58,59.] for different noble-transition metal nanoparticles, indicating that the lattice expands and contracts upon being treated in oxidizing (O_2) and reducing (H_2) atmospheres, respectively. We believe that the different support could also influence the overall oxophilicity of the AuPd catalysts.

For catalytic propane oxidation, oxygen activation is believed to play a major role in achieving the synergistic enhancement of the activity at n ~ 50. Since Au exhibits an immunity from oxidation in the nanoalloy under the reaction condition, it is possible that Au plays an important role in tuning surface sites but also the surface oxophilicity of Pd under the reaction temperature. In a study of CO oxidation over PdAu (synthesized by ~1:1 feeding ratio)/Al_2O_3 at 205 °C using combined XAFS/DRIFT measurements,[60] it was revealed that a stronger binding of CO on Pd atoms than Au lead to the formation of Pd shell and Au core. In another study of $Au_{88}Pd_{12}/TiO_2$ in the presence of CO/O_2 under reaction conditions,[61] a similar core-shell evolution was also observed, leading to a rapid deactivation of the catalyst. For propane oxidation, no apparent deactivation for our AuPd catalysts at ~T_{50} was observed even after extensive thermochemical treatment under oxygen, especially for Au% ≤50. Based on our previous report,[17] we believe that a core-shell evolution was insignificant. This assessment is supported by the data for the high- and medium-Pd catalyst (Au ≤ 50) in the reaction temperature range (Fig. 4A-B and S3A, ESI†). For Au%>50 and under the reaction temperature above T_{50}, there may be a slight enrichment of Pd as a result of the diffusion from the Pd-rich core, which is consistent with the data for the low-Pd catalyst (Au%>50) in the high temperature range (Fig. 4C and S4B, ESI†). In a study,[62] of the reaction pathway of propane oxidation over Pt/Al_2O_3, the existence of SO_4^{2-} was found to facilitate breaking of carbon-carbon bonds causing alteration of the reaction pathway. In the DRIFTS study of the catalytic oxidative stream of propane Pd/Al_2O_3 and Pt/CeO_2/Al_2O_3,[20] it identified two main species, formate species (1390 and 1590 cm^{-1}) and monodentated carbonate species (1502 cm^{-1}); The formate is active on Pd/Al_2O_3 while the carbonate is active on Pd/CeO_2/Al_2O_3. In comparison, our detection of the higher amounts of carbonate and formate

species for the Pd-rich alloy (Pd_9Au_{91}/Al_2O_3) seems to reflect a combination of the activities of Pd/Al_2O_3 and $Pd/CeO_2/Al_2O_3$. Propane oxidation reaction mechanism depends strongly on the chemical nature of the metal and support, as well as additives.[20,63]

By analysis of the distribution of intermediate species among $Pd_{91}Au_9/Al_2O_3$, $Pd_{55}Au_{45}/Al_2O_3$, and $Pd_{31}Au_{69}/Al_2O_3$ catalysts during propane reaction, there are clearly subtle differences in terms of the number of chemical or intermediate species and their diagnostic peak positions. For example, bicarbonate and acetate species were detected over $Pd_{91}Au_9/Al_2O_3$ and $Pd_{55}Au_{45}/Al_2O_3$ but not over $Pd_{31}Au_{69}/Al_2O_3$. Ester species were detected over $Pd_{91}Au_9/Al_2O_3$ but not over $Pd_{55}Au_{45}/Al_2O_3$. Based on the reaction steps proposed earlier for propane oxidation over Pd/Al_2O_3,[20] the some of the hypothesized reaction steps are considered for assessing the detection of the intermediate spices:

(1) Initial C-H bond cleavage by reacting with adsorbed O species followed by adsorption of $C_3H_{(8-n)}$ (n=1, 2, …)

e.g., $C_3H_8 + O_{ads.}$(on Pd site) $\rightarrow$ $C_3H_{(8-n)}$(ads.) + H_2O (ads)

(2) Reaction of activated $C_3H_{(8-n)}$ species with activated O species leading to cleavages of the first C-C bond and additional C-H bonds to form intermediate species.

e.g., $C_3H_{(8-n)}$(ads.) + O (ads) $\rightarrow$ *intermediate species* (e.g., ester, acetate, acetone, etc.)

(3) Reaction of the first-C-C bond cleaved intermediate species with activated O species leading to cleavages of the second C-C bond and additional C-H bonds to form intermediate species.

e.g., *first-C-C bond cleaved intermediate species* (e.g., ester, acetate, acetone, etc.) + O (ads) $\rightarrow$ *both C-C bond cleaved intermediate species* (e.g., bicarbonate, formate, etc.).

(4) Decomposition and release of the adsorbed intermediate species as CO_2 and H_2O.

Intermediate species $\rightarrow$ $CO_2 + H_2O$.

Based on previous reports,[16,18,60] C-H cleavage occurs with activated oxygen on catalyst surface from oxygen feed or provided form the support (Steps in (1)), which was considered to be rate determining step for propane oxidation.[64] Following the hydrocarbon cracking, the hydrocarbon fragments react with

activated oxygen species, forming first-C-C bond cleaved intermediate species (ester, acetate, acetone, etc.) and both C-C bond cleaved intermediate species (bicarbonate, formate, etc.) (Steps in (2) and (3)), which were detected over Pd_9Au_9 and $Pd_{55}Au_{45}/Al_2O_3$ with the relative abundances depending on the bimetallic composition. Further decomposition of oxy-carbon species, in oxidative environment lead to their release, forming CO_2 and H_2O (Steps in (4)).

To aid the understanding of the surface interactions and reactivities, DFT calculations using a small AuPd cluster model with 13 atoms were performed to assess the relative stability of the clusters and the adsorption energy of propane, O_2, and some intermediate species. Fig. 8 show the calculated adsorption energy for molecularly-adsorbed oxygen and propane, and intermediate acetate species on $Pd_{13-n}Au_n$ clusters. Details are summarized in Table S3,ESI†, along with additional calculation results for CH_3COO, $CH_3CH_2CH_2$, and CH_3CHCH_3 species on the cluster surfaces. The binding energy of the Au_nPd_{13-n} cluster follows the order of $Au_{13} < Pd_4Au_9 < Pd_7Au_6 < Pd_{12}Au_1 = Pd_{13}$, showing a decrease in binding energy as Au% increases (Table S4, ESI†).

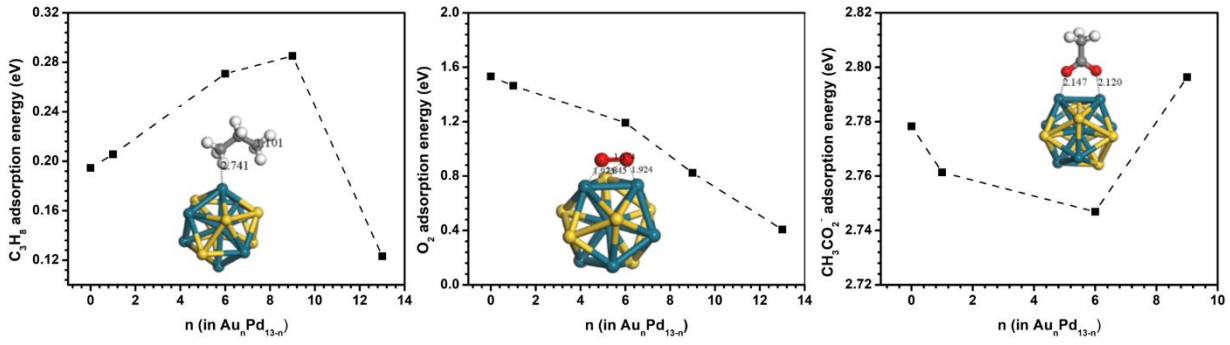

(A) **(B)** **(C)**

Fig. 8 DFT calculated adsorption energy for molecularly adsorbed propane (A), molecularly adsorbed oxygen (B), and adsorbed acetate (C) on $Pd_{13-n}Au_n$ clusters of different n values. Inserts: snapshots of the surface adsorption and cluster models.

As shown in Fig. 8A, the adsorption energy for propane on AuPd cluster model is very small, indicating very weak physical adsorption of propane on these clusters. In correlation with the experimentally-observed maximum activity for the catalyst with Pd:Au ~50, there is a maximum adsorption energy for propane over Pd_4 Au_9 and Pd_7 Au_6. Similarly, molecular adsorption of O_2 was evaluated based on Yeager model (Fig. 8B), revealing an intermediate adsorption energy for O_2 on Pd_7Au_6. The weak

interaction of O_2 and Au_{13} cluster was previously reported to result in a very low adsorption energy.[65] Interestingly, as shown Fig. 8C, it reveals a minimum adsorption energy of acetate species on Pd_7Au_6 cluster. In comparison with the weak but maximized adsorption energy for propane over Pd_7Au_6, there is a strong but minimized adsorption energy for intermediate acetate species over Pd_7Au_6. The calculated adsorption energy for acetate over Pd_7Au_6 is indeed very small, which suggest a weak adsorption of this species on the catalyst. However, the observed high DRIFTs intensity of acetate could suggest that acetate was relatively stable and underwent a slow conversion into CO_2.This correlation in combination with the intermediate adsorption energy for O_2 over Pd_7Au_6 is thus believed to be responsible for the experimentally-observed catalytic synergy in terms of the bimetallic composition. Note that the adsorption site features 2-fold Pd site for Pd_{13}, $Pd_{12}Au_1$, and Pd_7Au_6 clusters, while 2-fold Pd-Au site for Pd_4Au_9 cluster, suggesting the importance of Pd-Pd surface adsorption site near Au atoms for the catalytic synergy. It is important to note that the DFT result was based on a 13-atom cluster model due to limitation of our DFT calculation which, however, provides substantial information on the adsorption site and adsorption energy.

4. Conclusion

In conclusion, we have demonstrated for the first time that alloying Pd with Au in the catalyst with an optimal composition can enhance the catalytic activity for propane oxidation. The oxidation over $PdAu/TiO_2$ catalysts is shown to exhibit not only an enhanced catalytic activity, but also a strong composition dependence of the catalytic activity. The results have revealed not only an activity maximum at Pd:Au ~50:50 ratio in terms of reaction temperature, but also a composition-dependent sensitivity to the thermochemical treatment depending on the Au% in the NPs. The relative amounts of the non- or 1st C-C bond cleaved oxidation species (acetone, ester, and acetate) to complete (1st and 2nd) C-C bond cleaved oxidation species (formate, bicarbonate) depends strongly on the bimetallic composition. The activity maximum at Pd:Au ~50:50 ratio is believed to be linked to the weak but maximized adsorption energy for propane and strong but minimized adsorption energy for intermediate species, as well as the intermediate adsorption energy for O_2. While the activity for nanoalloys with n ~50 showed little change after the thermochemical treatment under oxygen, the activities for nanoalloys with $n < 50$ and $n > 50$ showed

opposite trend. In comparison with Pd-rich PdAu alloy on Al_2O_3, the absence of adsorbed formate and the reduced amount of adsorbed bicarbonate species Pd~50% PdAu alloy is linked to the higher activity in terms of achieving a complete C-C cleavage of propane towards CO_2 release. The combination of the lower surface oxophilicity in retaining the adsorbed intermediate formate and bicarbonate species and the increased lattice shrinking is believed to play an important role in the enhanced catalytic activity. It is also believed that the strong nanoalloy-support interaction for low- and medium-Au containing PdAu/TiO_2, constitutes the basis for the catalytic synergy, which, upon further probing of the surface sites, will provide new insights for the design of nanoalloy catalysts for low-temperature hydrocarbon oxidation.

Supporting Information.

The Supporting Information is available free of charge on the RSC Publications website: Additional HAADF-STEM image, catalytic activty data (Fig. S1-S4;), and DRIFTS data (Fig. S5-6; Table S1, and Table S2), and DFT calculation data (Table S3 and Table S4)

Conflicts of interest

There are no conflicts to declare

Acknowledgements

This work was supported by DOE-BES Grant (DE-SC0006877), the Department of Education Graduate Areas in National Need (GAANN), and the National Science Foundation Fund (CHE 1566283). Work at the Advanced Photon Source was supported by DOE under Contract DE-AC02-06CH11357. Thanks, are also due to 1-ID beamline staff for the help with the HE-XRD experiment.

References

1 M. Baldi, E. Finocchio and F. Milella, *Appl. Catal., B,* 1998**, 16**, 43-51.

2 C.-H. Lai, C.-C. Chang, C.-H. Wang, M. Shao, Y. Zhang and J.-L. Wang, *Atmos. Environ.,* 2009**, 43**, 1456-1463.

3 J. J. Spivey, *Ind. Eng. Chem. Res.,* 1987**, 26**, 2165-2180.

4 S. C. Kim and W. G. Shim, *Appl. Catal., B,* 2009**, 92**, 429-436.

5 D. Papageorgopoulos, M. Keijzer, J. Veldhuis and F. De Bruijn, *J. Electrochem*. Soc., 2002**, 149**, 1400-1404.

6 W. S. Epling and G. B. Hoflund, *J. Catal.* 1999**, 182**, 5-12.

7 D. M. Fernandes, C. F. Scofield, A. A. Neto, M. J. B. Cardoso and F. M. Z. Zotin, *Process Saf. Environ*., 2009, **87**, 315-322.

8 R. Fang, Y. Cui, Z. Shi, M. Gong and Y. Chen, *Chin. J. Catal.,* 2015, **36**, 994-1000.

9 C.-W. Yi, K. Luo, T. Wei and D. Goodman, *J. Phys. Chem. B*, 2005, **109**, 18535-18540.

10 X. Y. Lang, H. Guo, L. Y. Chen, A. Kudo, J. S. Yu, W. Zhang, A. Inoue and M. W. Chen, *J. Phys. Chem. C*, 2010, **114**, 2600-2603.

11 S. Xie, J. Deng, S. Zang, H. Yang, G. Guo, H. Arandiyan and H. Dai, *J. Catal.*, 2015, **322**, 38-48.

12 P. Yu, M. Pemberton and P. Plasse, *J. Power Sources*, 2005, **144**, 11-20.

13 C. Descorme, R. Taha, N. Mouaddib-Moral and D. Duprez, *Appl. Catal. A*, 2002, **223**, 287-299.

14 K. Okumura, T. Kobayashi, H. Tanaka and M. Niwa, *Appl. Catal., B,* 2003**, 44**, 325-331.

15 H. Yoshida, Y. Yazawa and T. Hattori, *Catal. Today,* 2003**, 87**, 19-28.

16 M. B. Griffin, A. A. Rodriguez, M. M. Montemore, J. R. Monnier, C. T. Williams and J. W. Medlin, *J. Catal.*, 2013, **307**, 111-120

17 H. Kareem, S. Shan, F. Lin, J. Li., Z. Wu, B. Prasai, C. P. O'Brien, I. C. Lee, D. T. Tran and L. Yang, *Nanoscale,* 2018, **10**, 3849-3862.

18 B. Wang, X. Wu, R. Ran, Z. Si and D. Weng, *Journal of Mol. Catal. A: Chem.* 2012**, 356**, 100-105.

19 C. P. O'Brien and I. C. Lee. *J. Catal.* 2017**, 347,** 1-8.

20 W. L. Faria, C. A. Perez, D. V. César, L. C. Dieguez and M. Schmal, *Appl. Catal., B,* 2009**, 92**, 217-224.

21 Ö. Metin, X. Sun and S. Sun, *Nanoscale* 2013, **5**, 910-912.

22 R. Loukrakpam, J. Luo, T. He, Y. Chen, Z. Xu, P. N. Njoki, B. N. Wanjala, B. Fang, D. Mott and J. Yin. *J. Phys. Chem. C,* 2011, **115,** 1682-1694.

23 S. M. Oxford, P. L. Lee, P. J. Chupas, K. W. Chapman, M. C. Kung and H. H. Kung, *J. Phys. Chem. C,* 2010, **114**, 17085–17091.

24 Egami, T.; Billinge, S.J. L. *Underneath the Braggs' Peak* (Pergamon/Amsterdam, Netherlands, 2003)

25 S. Krishnamurthy, A. Esterle, N. C. Sharma and S. V. Sahi, *Nanoscale res. let.* 2014**, 9**, 627.

26 V. Petkov, B. Prasai, S. Shastri, J.-W. Kim, S. Shan, H. R. Kareem, J. Luo and C. J. Zhong, *J. Phys. Chem. C*, 2017, **121**, 7854-7866.

27 S. Sakthivel, M. Shankar, M. Palanichamy, B. Arabindoo, D. Bahnemann and V. Murugesan, *Water res.*, 2004, **38**, 3001-3008.

28 S. Poulston, T. I. Hyde, H. Hamilton, O. Mathon, C. Prestipino, G. Sankar and A. W. Smith, *Phys. Chem. Chem. Phys.*, 2010, **12**, 484-491.

29 K. LeeáTan, *J. Mater. Chem.*, 2001, **11**, 2378-2381.

30 S. L. Hemmingson and C. T. Campbell, *ACS nano*, 2017, **11**, 1196-1203.

31 K. H. Hansen, T. Worren, S. Stempel, E. Lægsgaard, M. Bäumer, H.-J. Freund, F. Besenbacher and I. Stensgaard, *Phys. Rev. let.*, 1999, **83**, 4120.

32 C. T. Campbell and Z. Mao, *ACS Catalysis*, 2017, **7**, 8460-8466.

33 H. T. Li, L. F. Chen, X. Yuan, W. Q. Zhang, J. R. Smith and A. G. Evans, *J. Am. Ceram. Soc.*, 2011, **94**.

34 H. Chen, P. Li, N. Umezawa, H. Abe, J. Ye, K. Shiraishi, A. Ohta and S. Miyazaki, *J. Phys. Chem. C*, 2016, **120**, 5549-5556.

35 M. Ahmadi, F. Behafarid and B. R. Cuenya, *Nanoscale*, 2016, **8**, 11635-11641.

36 S. Tosoni and G. Pacchioni, *J. Phys. Chem. C*, 2017, **121**, 28328-28338.

37 S. Shan, V. Petkov, L. Yang, J. Luo, P. Joseph, D. Mayzel, B. Prasai, L. Wang, M. Engelhard and C. J. Zhong, *J. Am. Chem. Soc.*, 2014, **136**, 7140-7151.

38 M. N. Taylor, W. Zhou, T. Garcia, B. Solsona, A. F. Carley, C. J. Kiely and S. H. Taylor, *J. catal.*, 2012, **285**, 103-114

39 T. Maillet, C. Solleau, J. Barbier Jr and D. Duprez, *Appl. Catal. B Environ*, 1997, **14**, 85-95.

40 M. Li, D. Weng, X. Wu, J. Wan and B. Wang, *Catal. today*, 2013, **201**, 19-24.

41 Y. Li, X. Wang and C. Song, *Catal.Today*, 2016, **263**, 22-34

42 V. Petkov, Y. Maswadeh, A. Lu, S. Shan, H. Kareem, Y. Zhao, J. Luo, C. J. Zhong, K. Beyer and K. W. Chapman, *ACS appl. mater. interfaces*, 2018, **10**, 10870-10881.

43 B. D. Mukri, G. Dutta, U. V. Waghmare and M. Hegde, *Chem. Mater.*, 2012, **24**, 4491-4502.

44 Z. Ren, Z. Wu, W. Song, W. Xiao, Y. Guo, J. Ding, S. L. Suib and P.-X. Gao, *Appl. Catal., B,* 2016**, 180**, 150-160.

45 M. Skotak, Z. Karpiński, W. Juszczyk, J. Pielaszek, L. Kępiński, D. Kazachkin, V. Kovalchuk and J. d'Itri, *J. Catal.,* 2004**, 227**, 11-25.

46 G. Saracco, F. Geobaldo and G. Baldi, *Appl. Catal. B Environ.,*1999**, 20**, 277-288.

47 C.-W. Tang, L.-C. Hsu, S.-W. Yu, C.-B. Wang and S.-H. Chien, *Vib. Spectrosc.,* 2013**, 65**, 110-115.

48 H. Deng, Y. Yu and H. He, *J. Phys. Chem. C,* 2015**, 119**, 3132-3142.

49 Z. D. Yigezu and K. Muthukumar, *J. Anal. Appl. Pyrol.* 2015**, 114**, 60-67.

50 Van den Brand, O. Blajiev, P. Beentjes, H. Terryn and J. De Wit, *Langmuir,* 2004**, 20**, 6318-6326.

51 D. G. Rethwisch and J. Dumesic, *Langmuir***, 1986, 2**, 73-79.

52 V. Ermini, E. Finocchio, S. Sechi and S. Rossini, *Appl. Catal. A,* 2000**, 190**, 157-167.

53 A. R. McInroy, D. T. Lundie, J. M. Winfield, C. C. Dudman, P. Jones and D. Lennon., *Langmuir,* 2005, **21**, 11092-11098.

54 E. Finocchio, G. Busca, V. Lorenzelli and R. J. Willey, *J. Chem. Soc., Faraday Trans*, 1994, **90**, 3347-3356.

55 V. Petkov, S. Shan, P. Chupas, J. Yin, L. Yang, J. Luo and C. J. Zhong, *Nanoscale*, 2013, **5**, 7379-7387.

56 S. Shan, V. Petkov, L. Yang, D. Mott, B. N. Wanjala, F. Cai, B. H. Chen, J. Luo and C. J. Zhong, *ACS Catal.*, 2013, **3**, 3075-3085

57 E. Ozensoy, D. Herling and J. Szanyi, *Catal. Today,* 2008**,** 136, 46-54.

58 J. Wan, R. Ran, M. Li, X. Wu and D. Weng., *J. Mol. Catal. A-Chem.* **2**014**, 383**, 194-202.

59 Y. Yu, H. He, X. Zhang and H. Deng, *Catal. Sci. Technol.* 2014**, 4**, 1239-1245.

60 E. K. Gibson, A. M. Beale, C. R. A. Catlow, A. Chutia, D. Gianolio, A. Gould, A. Kroner, K. M. Mohammed, M. Perdjon and S. M. Rogers, *Chem. Mater.* 2015**, 27**, 3714-3720.

61 L. Delannoy, S. Giorgio, J. G. Mattei, C. R. Henry, N. El Kolli, C. Méthivier and C. Louis., *ChemCatChem,* 2013**, 5**, 2707-2716.

62 A. Hinz, M. Skoglundh, E. Fridell and A. Andersson, *J. Catal.,* 2001**, 201**, 247-257.

63 M. Hasan, M. Zaki and L. Pasupulety, *J. Phys. Chem. B,* 2002**, 106**, 12747-12756.

64 H. Luo, X.-D. Wu, D. Weng, S. Liu and R. Ran. *Rare Metals,* 2017**, 36**, 1-9.

65 F. Shojaei, M. Mousavi, F. Nazari and F. Illas, *Phys. Chem. Chem. Phys.,* 2015**, 17**, 3659-3672.

TOC Graphic:

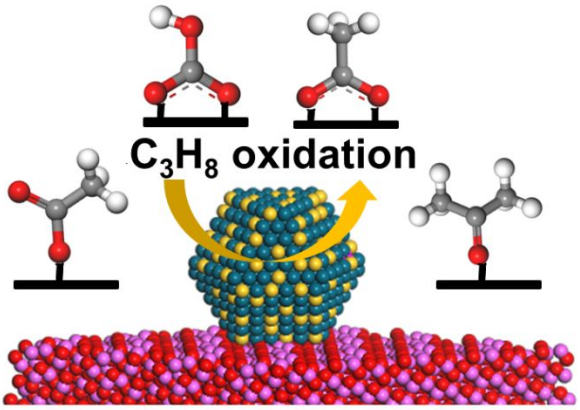

The surface intermediate species for the catalytic oxidation of propane over bimetallic nanoalloy catalysts depend strongly on the composition